SUPPLEMENTAL MATERIAL

Atlas of the immune cell repertoire in mouse atherosclerosis defined by single-cell RNA-sequencing and mass cytometry.

Holger Winkels[1*], Erik Ehinger[1*], Melanie Vassallo[1], Konrad Buscher[1], Huy Dinh[1], Kouji Kobiyama[1], Anouk A.J. Hamers[1], Clément Cochain[2], Ehsan Vafadarnejad[3], Antoine-Emmanuel Saliba[3], Alma Zernecke[2], Akula Bala Pramod [1], Amlan Ghosh[1], Nathaly Anto Michel[4], Natalie Hoppe[4], Ingo Hilgendorf[4], Andreas Zirlik[4], Catherine C. Hedrick[1], Klaus Ley[1†], and Dennis Wolf[1,4†]

Affiliations:
[1] La Jolla Institute for Allergy and Immunology, Division of Inflammation Biology, La Jolla, CA, USA
[2] Institute of Experimental Biomedicine, University Hospital Würzburg, Würzburg, Germany
[3] Helmholtz Institute for RNA-based Infection Research, Würzburg, Germany
[4] Department of Cardiology and Angiology I, University Heart Center Freiburg, and the Faculty of Medicine, University of Freiburg, Freiburg, Germany

CONTENT

ONLINE MATERIAL AND METHODS

Data availability. All data and methods used in the analysis, and materials used to conduct the research will be made available to any researcher for the purpose of reproducing the results or replicating the procedures. All data, methods, materials are available upon personal request at the La Jolla Institute for Allergy and Immunology, CA, USA (contact: dwolf@lji.org).

Mice. All experiments followed guidelines of the La Jolla Institute for Allergy and Immunology (LJI) Animal Care and Use Committee. Approval for use of rodents was obtained from LJI according to criteria outlined in the Guide for the Care and Use of Laboratory Animals from the National Institutes of Health. *Apoe*$^{-/-}$ mice on a C57BL/6J background were maintained in-house on a 12-hour light/dark cycle. For atherosclerosis studies, 8-week old female *Apoe*$^{-/-}$ mice were fed a standard chow diet (CD) or a western-type diet (WD) containing 0.2% cholesterol (Envigo, TD.88137) for 12 weeks. Alternatively, mice at the age of 8 weeks or *Ldlr*$^{-/-}$ mice after feeding with a high cholesterol diet (HCD) for 12 weeks were used. Mice were euthanized by CO_2 inhalation. As indicated, splenocytes from CD45.1 *Apoe*$^{-/-}$ mice served as controls.

Aorta Collection and Processing. Aortas were digested as previously described[1]. Surgically excised aortas were collected in 1ml RPMI media (Gibco) containing 10 % fetal calf serum (FCS) on ice. Aortas were then cut into small pieces and individually digested for 1 hour at 37° C in HBSS containing 450 U/mL Collagenase I (Sigma Aldrich), 250 U/mL Collagenase XI (Sigma Aldrich), 120 U/mL Hyaluronidase (Sigma Aldrich), and 120 U/mL DNase I (Worthington). The digested aortic suspension was subsequently filtered through a 50 μm cell strainer (Partec) and washed with 37° C pre-warmed 10 % FBS/RPMI (5 min, 500 g). Cells were kept in 10% FBS/RPMI for 30 minutes at 37° C in a cell culture incubator to allow for the recovery of cell surface molecule expression affected by digestion.

Histochemistry and morphology. Aortas were excised and separated into three parts: (1) the arch, (2) the thoracic part from below the arch to the renal aortas, and (3) the abdominal aorta from below the renal aortas to the aortic bifurcation. All parts were embedded in OCT Tissue TEK and cut into 10 µm-thick serial sections with a cryostat. Serial sections were stained with hematoxylin and eosin (H&E) or Oil-Red-O (Sigma) to determine cellularity and lipid depositions, respectively. Sections were imaged with the automatic slide scanner Axio Scan.Z1 (Zeiss) equipped with a computerized morphometry system (Zen pro, Zeiss). For the staining, air-dried cryostat sections were pre-incubated with 60% 2-propanol by 10-times dipping the sections in the solution and subsequently kept 15 minutes in the Oil-Red-O-working solution (180 ml Oil red O-stock solution and 120 ml distilled water filtered 1 hour after mixing to remove precipitated salts). Excess Oil-Red-O solution was washed out by dipping 10-times in 60 % 2-propanol. The sections were rinsed twice for 5 minutes with tap water and Oil-red-O-stained sections were embedded in Immu-Mount (Thermo Scientific). Tissue sections with insufficient staining quality were excluded from further analysis.

Human plaque processing and cell isolation. Human carotid plaques were collected from patients undergoing carotid endarterectomy with an approval by the local Institutional Review Board at the University of Freiburg, Germany. The atherosclerotic plaque was cut into small pieces with a razorblade. Subsequently, tissue pieces were digested for 1 hour at 37° C in HBSS containing 200 U/ml DNase I (Sigma) and 250 U/ml Collagenase IV

(Sigma). The digested plaque cell suspension was filtered through a 50 μm cell strainer (Partec), calcified parts were removed, and the cell suspension was washed with 37° C pre-warmed RPMI supplemented with 10 % human serum (5 minutes, 500 g). Cells were kept in 10 % human serum/RPMI for 30 minutes at 37° C in a cell culture incubator to allow for the recovery of cell surface molecule expression affected by digestion. Cells were subsequently processed for CyTOF and data were analyzed using the same methodology as described for mouse samples.

Splenocyte isolation. Splenocytes were isolated by pushing spleens through a 70 μm cell strainer (BD Biosciences), followed by a wash with PBS and red blood cell lysis for 3 minutes (eBioscience). Splenocytes were washed several times in PBS, and the cell concentration was adjusted to 1 x 10^6/ml in PBS. One million splenocytes from CD45.1 *Apoe*$^{-/-}$ mice were added to aortic cell suspension (CD45.2) to increase the cell number and detection yield during mass cytometry data acquisition.

Conventional flow cytometry. Aortic single cell suspensions were incubated with fluorochrome-coupled antibodies against the following antigens for 20 minutes at 4° C: CD45, CD11b, F4/80, TCR-γ/δ, CD117 (c-Kit), CD19, FcεR1, CD11c, NK1.1, TCR-β, Ly-6C/G (Gr-1), CD4, and CD8. The antibody incubation buffer contained 10 % rat serum and 10 μg/ml of an anti-CD16/CD32 antibody. Clones and concentrations used are listed in Online-Table II and IX. After incubation, cells were washed several times and fixed with 2% Paraformaldehyde (PFA) for 10 minutes. Cells were washed, resuspended in PBS containing 2% FBS, and acquired on a LSRII flow cytometer (BD Biosciences).

Intracellular cytokine staining. Aortic single cell suspensions were incubated with protein transport inhibitor cocktail and cell stimulation cocktail (eBioscience) for 5 hours and stained with fluorochrome-coupled antibodies against the following antigens for 20 minutes at 4° C: CD45, CD19, CD43, and B220. Antibody clones are listed in Online-Table XIII. The antibody incubation buffer contained 10 % rat serum and 10 μg/ml of an anti-CD16/CD32 antibody. After incubation, cells were washed and fixed with 2 % Paraformaldehyde (PFA) for 30 minutes. Cells were washed twice with 1x permeabilization buffer (eBioscience) and stained with fluorochrome-conjugated antibodies against IL-10, IL-4, IFN-γ, GM-CSF, and CCL5 for 30 minutes at room temperature. Cells were washed, resuspended in PBS containing 2 % FBS, and acquired on a LSRII flow cytometer (BD Biosciences).

Mass cytometry antibody conjugation. For mass cytometry antibody staining, directly conjugated antibodies were purchased from Fluidigm. Alternatively, purified antibodies (Online-Tables VI and IX) were labelled with the Maxpar X8 Multi-Metal Labeling Kit (Fluidigm) according to the manufacturer's instructions. Conjugation efficiency was verified by NanoDrop One/One^c (ThermoFisher) and binding to CompBead Plus antibody capture beads (BD Biosciences). All antibody concentrations were titrated.

Mass cytometry (CyTOF). For viability staining, cells were washed in PBS and stained with Cisplatin (Fluidigm) to a final concentration of 5 μM. Cells were washed and stained with the antibody cocktail listed in Online-Table II. Antibodies were prepared in staining buffer (PBS with 2 mM EDTA, 0.1 % BSA, 0.05 % NaN_3). After staining, cells were washed and fixed with 2 % paraformaldehyde (PFA) overnight at 4° C. After fixation, cells were washed in staining buffer and permeabilized using 1x Permeabilization Buffer (eBioscience). For cell identification, cells were washed in staining buffer and stained with

DNA intercalator (Fluidigm) containing natural abundance Iridium (^{191}Ir and ^{193}Ir) prepared to a final concentration of 125 nM in 2% PFA. Cells were washed in staining buffer and Milli-Q water (EMD Millipore) to remove buffer salts. Cells were next resuspended in Milli-Q water with a 1:10 dilution of EQ Four Element Calibration beads (Fluidigm) and filtered through a 35 μm nylon mesh filter cap (Corning). Samples were acquired on a Helios CyTOF Mass Cytometer (Fluidigm) at an event rate of 500 events/second or less using a Super Sampler (Victorian Airship & Scientific Apparatus LLC). Data was normalized (including EQ bead-removal) using Matlab-based normalization software[2]. After gating on DNA intercalator double-positive events, aorta and spleen samples were separated by manually gating on live CD45.2$^+$ (aorta) and CD45.1$^+$ cellular events (spleen).

Unsupervised leukocyte clustering in flow- and mass cytometry. To detect clusters of cells with a similar expression of cell surface markers in FACS or CyTOF, live CD45$^+$ leukocytes were gated, and selected marker expression on a single cell level was clustered using the unsupervised dimensionality reduction algorithm t-Distributed Stochastic Neighbor Embedding (tSNE) algorithm[3] in Cytobank (1,000 iterations, Perplexity 30, Theta 0.5). The final KL divergence was 1.849. Additionally, live CD45$^+$ events were exported as new FCS files and imported into the R/Bioconductor environment (v3.3.3) using the cytofkit package (v1.6.6)[4]. Clustering was performed using default settings (k=30) of the PhenoGraph implementation in the cytofkit package by reading the viable CD45$^+$ FCS files. All events and all markers, aside from CD45 and the viability stain, were included for clustering analysis. Data was not transformed prior to clustering. Simultaneously, the tSNE algorithm was applied (6,000 iterations, perplexity 30, theta 0.5) including the same markers as PhenoGraph. Visualization of mass cytometry data was performed using shinyAPP. The resulting PhenoGraph clusters were projected onto the CD45$^+$ t-SNE map. Frequencies of all leukocyte clusters per mouse were exported from the R/Bioconductor environment, and a heatmap normalized for each marker within all generated clusters was created with the web-based tool Morpheus (GenePattern, Broad Institute), using the marker mean-fluorescence expression (MFI) values from each cluster. Clusters were then manually assigned to known hematopoietic lineages by typical marker expression.
For CyTOF data analysis, only marker expression from CD45.2$^+$ cellular events was transformed using the Arcsinh method. Simultaneously, the tSNE algorithm was applied (6,000 iterations, perplexity 30, theta 0.5) including the same markers used in PhenoGraph. Visualization of mass cytometry data was performed using shinyAPP (integrated into the cytofkit package). The resulting PhenoGraph clusters were projected onto the CD45$^+$ tSNE map. The frequencies of all leukocyte clusters per mouse were exported from the R/Bioconductor environment. In addition, the average of Arcsinh for each cluster was exported from R, and a row-normalized heatmap was generated using the web-based tool Morpheus (GenePattern, Broad Institute).

CyTOF marker-expression categories. To classify the expression signal of a given marker in a cell cluster identified in CyTOF experiments, we applied the following 2 strategies: (1) Marker expression was classified based on expression peaks identified in marker-histograms: When a marker appeared in four different, distinct expression peaks within one leukocyte lineage, we named these high-, med-, low-, and negative-expressed with a descending marker signal in this order. For instance, this applied to CD5. In the case of three different expression levels, we named these high-, low-, and negative, which applied to CD4. In the case of two distinct expression levels, we named these high-, and negative, which applied to FR4. This relative categorization of marker expression intensity is only valid within one hematopoietic leukocyte lineage and does not allow to compare

absolute signal values of the same expression-category across different leukocyte lineages. Examples for this strategy are shown in Online-Figure XIII. (2) If the expression signal of a marker was not confined to one peak only, e.g. in the case of a mixed population with neg-, low-, and high-expressing cellular events, we tested the mean signal strength of the population and assigned the population to an averaged neg-, low-, med-, or high-expression level (Figure 4) for clarity.

Sorting for single cell RNA-sequencing. A CD45-BV510 antibody (clone 30-F11, Biolegend) was injected i.v. into mice 5 minutes before sacrifice to specifically label circulating leukocytes. Aortas were excised and processed as described above. Aortic single cell suspensions of individual mice were combined according to diet as indicated. The resulting cell suspension was stained with Viability Dye BV506 (Tonbo Biosciences), Ter119-BV510 (clone TER-119, Biolegend), and CD45-PerCp (clone 30-F11, Biolegend). Viable aortic leukocytes (CD45-PercP^{+} L/D^{-}), excluding circulating leukocytes (CD45-BV510^{+}) and erythrocytes (TER-119^{+}), were sorted with a 100 μm nozzle using the BD FACSAria Fusion (BD Biosciences), collected in serum-free media (TexMACS Medium, Miltenyi), washed twice with PBS, and reconstituted in PBS containing 400 μg/ml ultra-pure bovine serum albumin (Ultrapure BSA, Ambion, AM2616) to 1x10^{6} cells/ml. Cell suspensions were kept in low absorbent micro-centrifuge tubes on ice. 8 μl cell suspension (~8000 cells) were loaded on one Chromium Single Cell controller chip (10xGenomics).

Single Cell RNA-sequencing (scRNAseq). Aortic leukocyte suspensions were loaded on the Chromium Single Cell Controller (10xGenomics) to generate a single cell and gel bead emulsion (GEM)[5]. ScRNAseq libraries were prepared using the Single Cell 3' Solution v2 Reagent Kit (10xGenomics). GEM reverse transcription was performed by the SimpliAmp thermal cycler (Thermo Fisher Scientific) running the following program: 53° C for 45 minutes and 85° C for 5 minutes; held at 4° C. Following reverse transcription, GEMs were broken, and single-strand cDNA was purified with DynaBeads MyOne Silane Beads (Thermo Fisher Scientific). cDNA was amplified with the SimpliAmp thermal cycler: 98° C for 3 minutes, 12 cycles of 98° C for 15 seconds, 67° C for 20 seconds, 72° C 60 seconds; 72° C for 1 minute, and held at 4° C. Subsequently, cDNA was cleaned up using the SPRIselect reagent kit (Beckman Coulter), quantified, and quality controlled with the Agilent Bioanalyzer High Sensitivity Kit. Indexed sequencing libraries were prepared by Single Cell 3' Solution v2 Reagent Kit's components: (1) enzymatic fragmentation, (2) end repair, (3) A-tailing, (4) adaptor ligation, (5) post ligation cleanup with the SRPIselect reagent kit, and (6) sample index PCR using the SimpliAmp thermal cycler at 98° C for 45 seconds, 10 cycles of 98° C for 20 seconds, 54° C for 30 seconds, 72° C for 20 seconds; 72° C for 1 minute, and held at 4° C. The SPRIselect reagent kit was used for post sample index double-sided size selection, and the library was quality controlled post construction using the Agilent Bioanalyzer High Sensitivity Kit and Agilent Bioanalyzer high sensitivity chip. The library was quantified post construction by quantitative PCR (Kapa DNA Quantification Kit for Illumina platforms). The constructed libraries were loaded at 13 pM on a HiSeq2500 Rapid Run using a HiSeq Rapid Cluster Kit V2- Paired End (PE), and a HiSeq Rapid SBS Kit V2. A 26-base-pair Read 1 was used to sequence the cell barcode and UMI, an 8 bp i7 index read was used to sequence the sample index, and a 98 bp Read 2 was used to sequence the transcript on an Illumina HiSeq4000 using paired-end sequencing with dual indexing.

ScRNAseq data analysis. 10x genomics single cell transcriptome sequencing data was processed using the Cell Ranger Single Cell software suite Version 1.3

(https://support.10xgenomics.com) as described previously[5]. Briefly, the FASTQ files were processed with the Cellranger count pipeline, which uses STAR[6] to align the reads to mm10 mouse reference transcriptome. The output cloupe file was visualized in the Loupe Cell Browser (10xGenomics) for the graph-based and K-means clusters of the single cell data. Dimensionality reduction was performed by the graph-based algorithm that precedes pre-filtering PCA-defining genes, followed by t-SNE. A k-means filtering[7] of K=12 was performed for the separation of the main aortic leukocyte populations. Single cell expression data and mean cluster transcript expression, as well as single cell expression heatmaps of differentially expressed genes, were extracted with the Cell Ranger R kit. UMI normalization was done by dividing UMI counts by the total UMI counts in each cell, followed by multiplication with the median of the total UMI counts across cells. Alternatively, raw data were processed with the R/Biodoncuctor single cell RNA-sequencing analysis package SEURAT[8]. Raw sequencing reads from the indicated samples were merged, the gene space was log-normalized, and filtered for the following parameters: unique gene count per cell >50 and <2500, percent of mitochondrial genes of all genes <0.05. A PCA-reduction (up to 12 dimensions) was performed and a Stochastic Neighbor Embedding (t-SNE) and automated cluster detection algorithm was performed on the gene sets defining the PCA variability. Only significant PCA-dimensions were taken into account. Cluster detection was run with resolution of 0.8 to 0.9. DE-genes between clusters (one cluster compared to all remaining) were defined by a T-test with a P<0.05.
Alternatively, for intra-population heterogeneity, *Cd19* mRNA-expressing cells from WD-fed *Apoe*$^{-/-}$ animals were selected using the SeqGeq genomic gating tool (Treestar Software) and filtered for the top 250 genes with the highest variance across all cells within this data set. This gene set was used as input for t-SNE with a perplexity of 7. K-means clustering on the 2D t-SNE plot was performed using an adapted algorithm that automatically determines the number of clusters based on a standard significance level[9]. Based on a significance of 0.2, 3 major populations were retrieved. Differentially expressed genes were then filtered with the Comparative Marker Suite (GenePattern, Broad Institute), with cutoffs for FDR<5% (Benjamini Hochberg) and p<0.05 (two-sided T-test, 10000 permutations) on the full gene set of all B cells in the 3 populations (one-versus-all comparison). Genes were displayed in column minimum-maximum value heatmaps generated by Morpheus (GenePattern, Broad Institute), followed by free hierarchical clustering (one-minus-pearson with average linkage).

Functional pathway analysis. Expression data from scRNAseq experiments were used to generate differentially expressed genes between t-SNE/K-means-derived clusters or manually gated single cell events. A p-value of <0.05 and a FDR of <0.05 served as cutoffs for significance between the groups. Significantly up-regulated genes between a group and all remaining groups were selected as the exclusively regulated genes per group. These genes served as input for pathway analysis by DAVID[10]. Significantly regulated functional clusters or single pathways were further grouped by the indicated functional classes and compared by the enrichment score. Alternatively, differentially expressed genes between aortic leukocytes from CD and WD-fed mice within the same scRNAseq cell clusters were uploaded to Qiagen IPA and processed using the Core Analysis function[11]. Up- and down-regulated genes were used in separate analyses in order to determine which pathways were enriched in western diet and/or in chow diet. Significantly enriched (p<0.05) canonical pathways were filtered and two top pathways for WD and CD were selected as representative enriched pathways. The top ten pathways for each cluster are shown in Online-Table V.

Gene set enrichment analysis. GenePattern 2.0[12] was used to process RNA array data for gene set enrichment analysis[13] which was run with the default settings (100 iterations, weighted). Gene enrichment was tested on human ruptured and stable human plaques (GSE41571)[14]. As signature gene sets, we used the top 50 DE-genes (highest fold change, $P<0.05$) from each individual leukocyte cluster. Enrichment was tested between ruptured and stable atherosclerotic plaques. A P-value<0.05 and a FDR<0.2 were considered significant.

Gene set score. To identify cell- or lineage specific gene expression on a single cell level we applied gene expression scores as previously described[15] and overlaid these color-coded on tSNE plots. Gene set scores were normalized to background to account for a different number of expressed genes.

Genetic deconvolution (GD). To estimate the frequency of leukocytes with a specific gene signature within a whole tissue RNA expression data set, we applied a genetic deconvolution strategy as previously described[16]. This method allows to robustly calculate the relative frequency of specific cellular gene signatures in bulk mRNA expression sets also containing non-$CD45^+$ cells and serves as a relative estimate for cellular frequencies. This method is comparable to previously published genetic deconvolution methods[17-22] and was validated for robustness, specificity, and sensitivity to detect leukocyte RNA 'hidden' in non-leukocyte RNA to allow the detection of leukocyte infiltrates in target tissues[16]. We applied a stepwise strategy to construct, validate, and use aortic leukocyte signatures for genetic deconvolution. These steps (shown in revised Online Figure VII a) included: (I) Identification of aortic leukocyte clusters in scRNAseq (Fig. 1) and comparison of the frequencies of principal hematopoietic lineages retrieved by this scRNAseq approach to those retrieved by conventional flow cytometry (Online Figure V). (II) Identification of the aortic leukocyte cluster identity by a GD of published mouse transcriptomes within the complete expression data set of each cluster[23] (Online Figure IV). (III) Construction of scRNAseq cluster gene signatures based on the top 50 DE-genes of each cluster (compared to all others). The specificity of these aortic cluster gene signatures was validated by a GD of the signatures within the complete gene-expression data set of each cluster (Online Figure VII b). (IV) A GD of aortic leukocyte cluster signatures within whole tissue mRNA expression data sets from LN, spleen, and blood mRNA from *Apoe*$^{-/-}$ mice (GSE40156) was performed and de-convoluted cluster frequencies were compared to de-convoluted frequencies of a published mouse PBMC gene signature[23] within the same data set. In addition, results were compared to the frequencies assessed by flow cytometry of leukocytes from the same locations (Online Figure VII c, d). (V) A GD of aortic leukocyte cluster signatures within microdissected aortic tissue mRNA (GSE21419, Figure 2) and whole aortic mRNA (GSE40156, Online Figure VII e) from atherosclerotic *Apoe*$^{-/-}$ mice was performed. Cluster frequencies were compared to the frequencies of published mouse transcriptomes[23]. (VI) A GD of mouse aortic leukocyte clusters was performed in human whole tissue mRNA from PBMCs and atherosclerotic plaques after endarterectomy[24] (Figure 7).

Statistics. For visualization and statistical testing of normally-distributed, continuous variables between two groups, an unpaired, two-sided Student's T-test was applied. Significances between multiple groups were assessed by a One-Way-ANOVA. Significant enrichments of different functional cytokine expression patterns were calculated by χ^2 test. For Kaplan-Maier survival analyses a Logrank and Gehan-Breslow-Wilcoxon test was applied. A P-value < 0.05 was considered significant. All data are presented as mean ± standard error of the mean (SEM).

ONLINE FIGURES

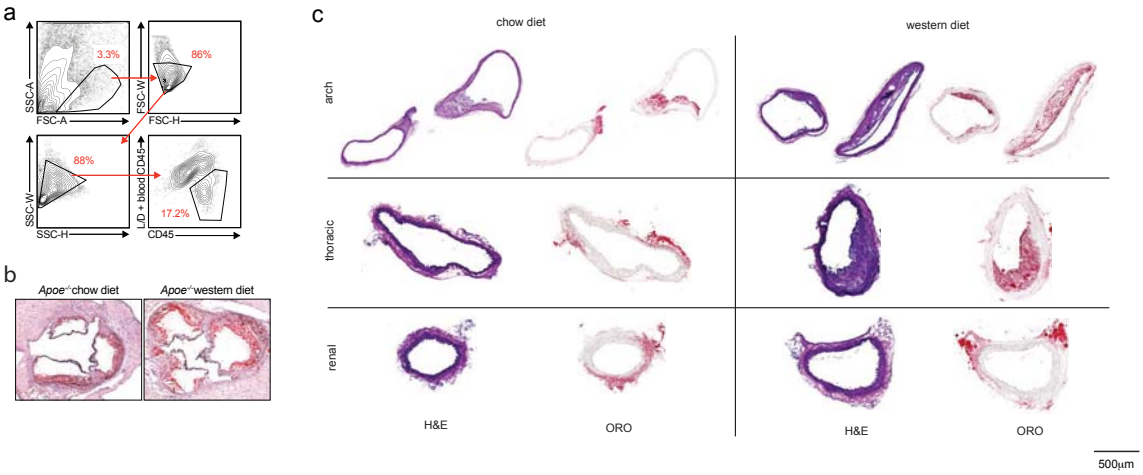

Online Figure I: Gating strategy for flow sorting of aortic leukocytes and representative immunohistochemistry of atherosclerotic plaques used for single cell RNA-sequencing. (**a**) Gating strategy to exclude contaminating blood leukocytes: An anti-CD45-BV510 antibody was injected i.v. 5 minutes prior to the excision of the aorta. (**b**) 8-week-old, female *Apoe*-deficient (*Apoe*$^{-/-}$) mice consumed either chow (CD) or western diet (WD) for 12 weeks. Cross-sections of the aortic arch, thoracic aorta, and abdominal aorta were stained hematoxylin and eosin (H&E) to display cellularity or Oil-Red-O (ORO) to assess plaque size. (**c**) 8-week old, male *Apoe*$^{-/-}$ mice consumed either a standard chow diet (CD) or a cholesterol-rich western diet (WD) for 12 weeks. The extent of atherosclerotic lesions was quantified in the aortic sinus by a lipid-specific Oil-red-O (ORO) stain.

a

	Baseline	CD	WD
Number of Cells	555	909	2077
Number of Reads	311,890,807	135,596,242	128,851,208
Mean Reads per Cell	561965	149170	62037
Median Genes per Cell	1004	1277	1133
Total Genes Detected	13692	14518	15279
Median UMI Counts per Cell	2940	3722	3177
Valid Barcode	98.0%	98.2%	98.1%
Reads Mapped Confidently to Transcriptome	57.0%	64.6%	62.0%
Reads mapped Confidently to Exonic Regions	60.1%	67.8%	65.3%
Reads Mapped Confidently to Intronic Regions	17.9%	19.0%	19.3%
Reads mapped Confidently to Intergenic Regions	4.7%	3.5%	3.7%
Sequencing Saturation	98.4%	93.6%	87.2%
Q30 Bases in barcode	98.2%	96.3%	96.3%
Q30 Bases in RNA Read	82.6%	87.9%	86.5%
Q30 Bases in UMI	98.3%	97.0%	97.8%

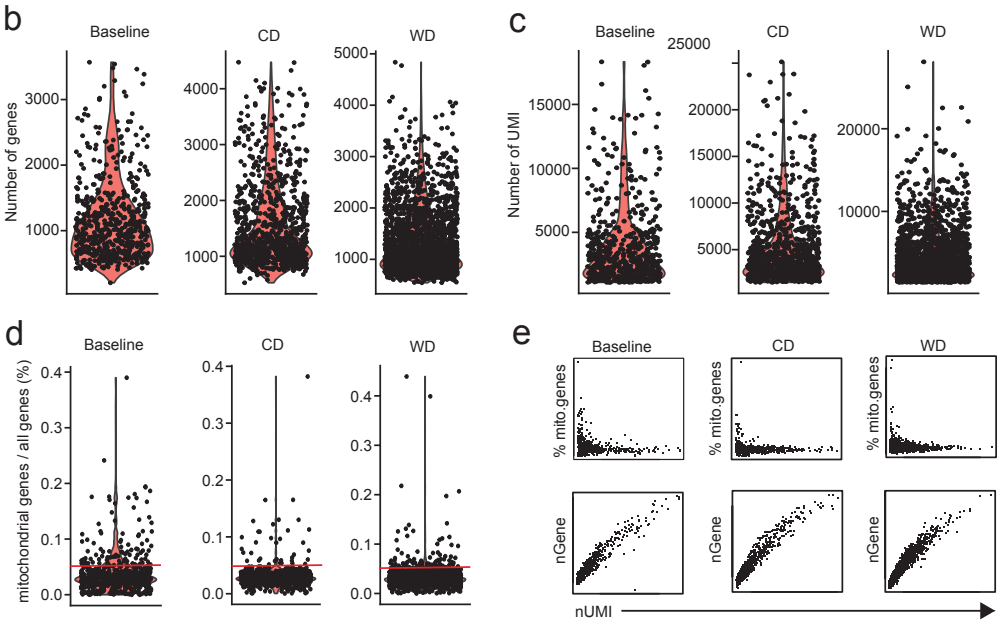

Online Figure II: Quality controls for single-cell RNA-sequencing (scRNAseq) of aortic leukocytes. (**a**) Sequencing parameters from single cell leukocyte suspensions subjected to the Chromium/10xGenomics scRNAseq platform. Leukocytes were isolated from 8-week old *Apoe*$^{-/-}$ mice (baseline), 20-week old *Apoe*$^{-/-}$ mice fed chow diet (CD), and 20-week old *Apoe*$^{-/-}$ mice fed western-type diet (WD) for 12 weeks. (**b**) Number of genes for single cells within each data set/cell suspension. Cells within a gene number between 50-2500 were included. (**c**) Number of unique molecular identifier (UMI) per cell for each data set/cell suspension. (**d**) Percentage of mitochondrial genes/all genes (expressed as %) within individual single cell transcriptomes for the respective dataset. A cutoff was set to 0.05 % mitochondrial genes/total genes (indicated by a red line). (**e**) % mitochondrial genes/all genes per cell (% mito.genes) and total number of genes per cell (nGene) in relation to UMI counts are shown.

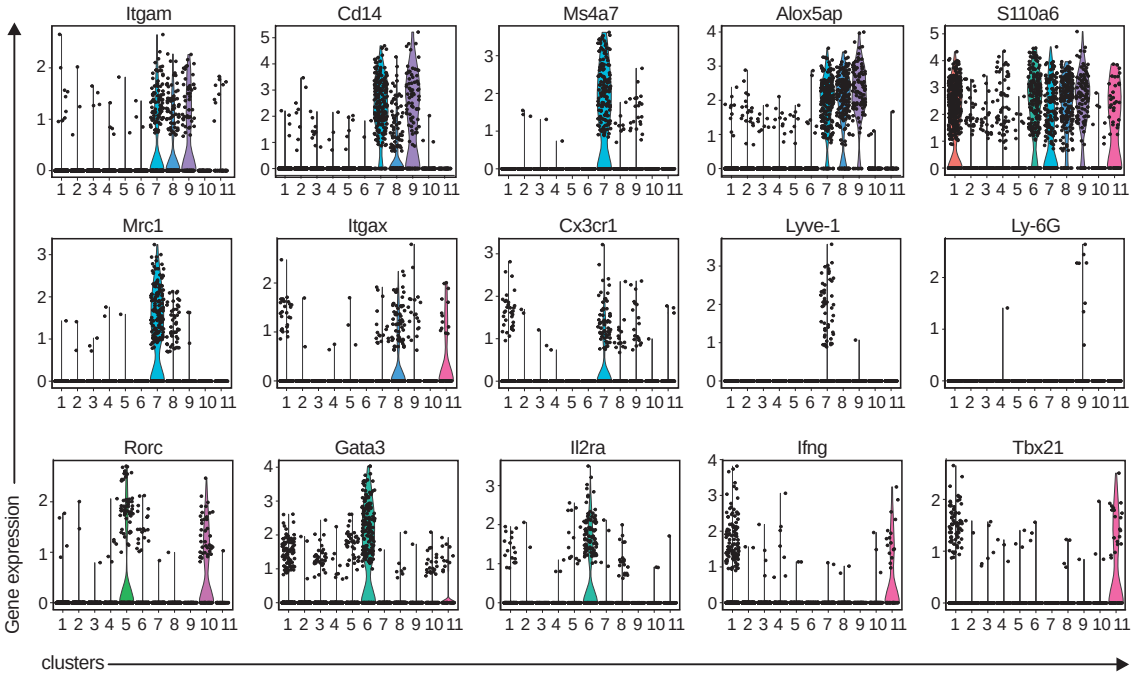

Online Figure III: Single cell gene expression of mouse leukocyte lineage markers. Aortic leukocytes were isolated, subjected to scRNAseq, and distinct leukocyte clusters in CD and WD-fed mice (*Apoe*$^{-/-}$ mice at a total age of 20 weeks after 12 weeks feeding) were identified by dimensionality reduction of single cell transcriptomes. Single cell gene expression (normalized) per cell is shown in violin plots. Cluster number according to Figure 1.

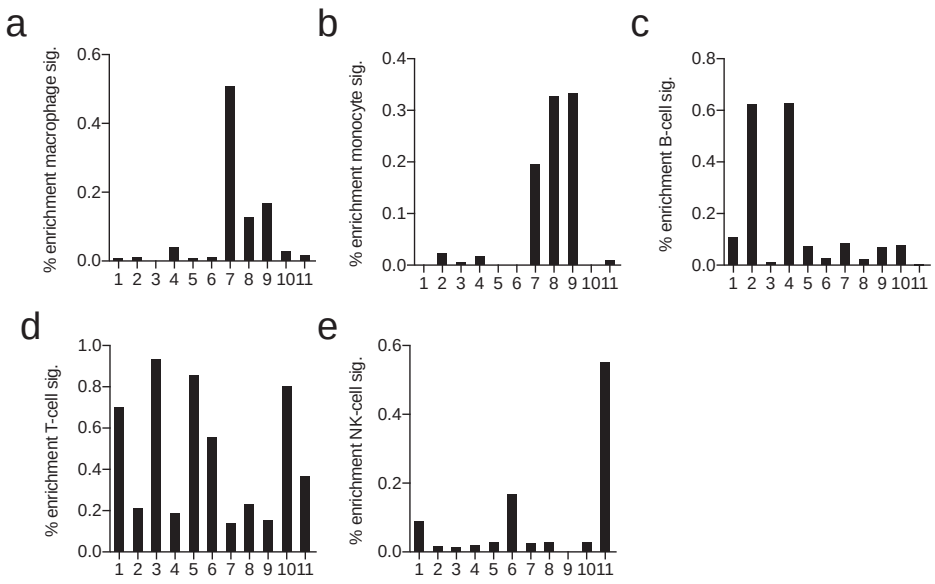

Online Figure IV: Identification of cluster identities. Aortic leukocytes were isolated, subjected to scRNAseq, and distinct leukocyte clusters in CD and WD-fed mice (*Apoe*$^{-/-}$ mice at a total age of 20 weeks after 12 weeks feeding) were identified by dimensionality reduction of single cell transcriptomes. Cluster transcriptomes were tested in a genetic deconvolution strategy to published mouse PBMC transcriptomes (macrophages / monocytes / B-cells / T-cells / Nk-cells). Percentage of identified signature within the cluster transcriptome (% enrichment / tested signature) is shown.

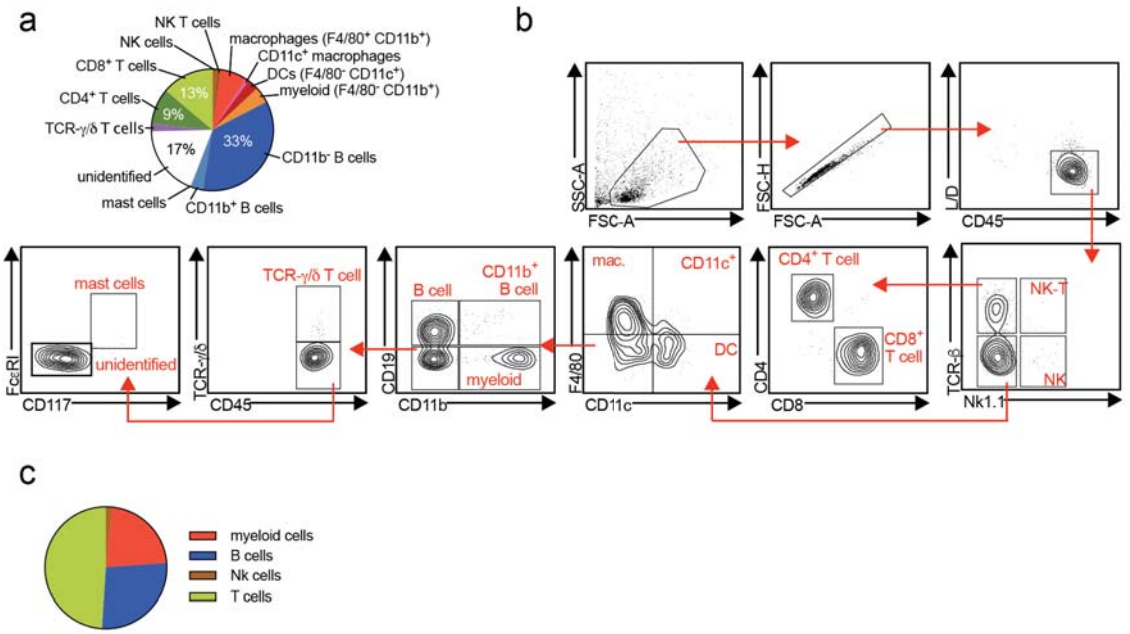

Online Figure V: Flow cytometry to identify principal hematopoietic lineages in the mouse aorta. (**a**) Relative abundance of aortic leukocyte populations in *Apoe*$^{-/-}$ mice (n=10) fed a WD for 12 weeks (expressed as % of all viable leukocytes). (**b**) Boolean gating strategy to identify hematopoietic lineage commitment of aortic leukocytes. (**c**) Frequencies of principal hematopoietic lineages found by scRNAseq (Figure 1) were grouped and shown as relative frequency of all leukocytes.

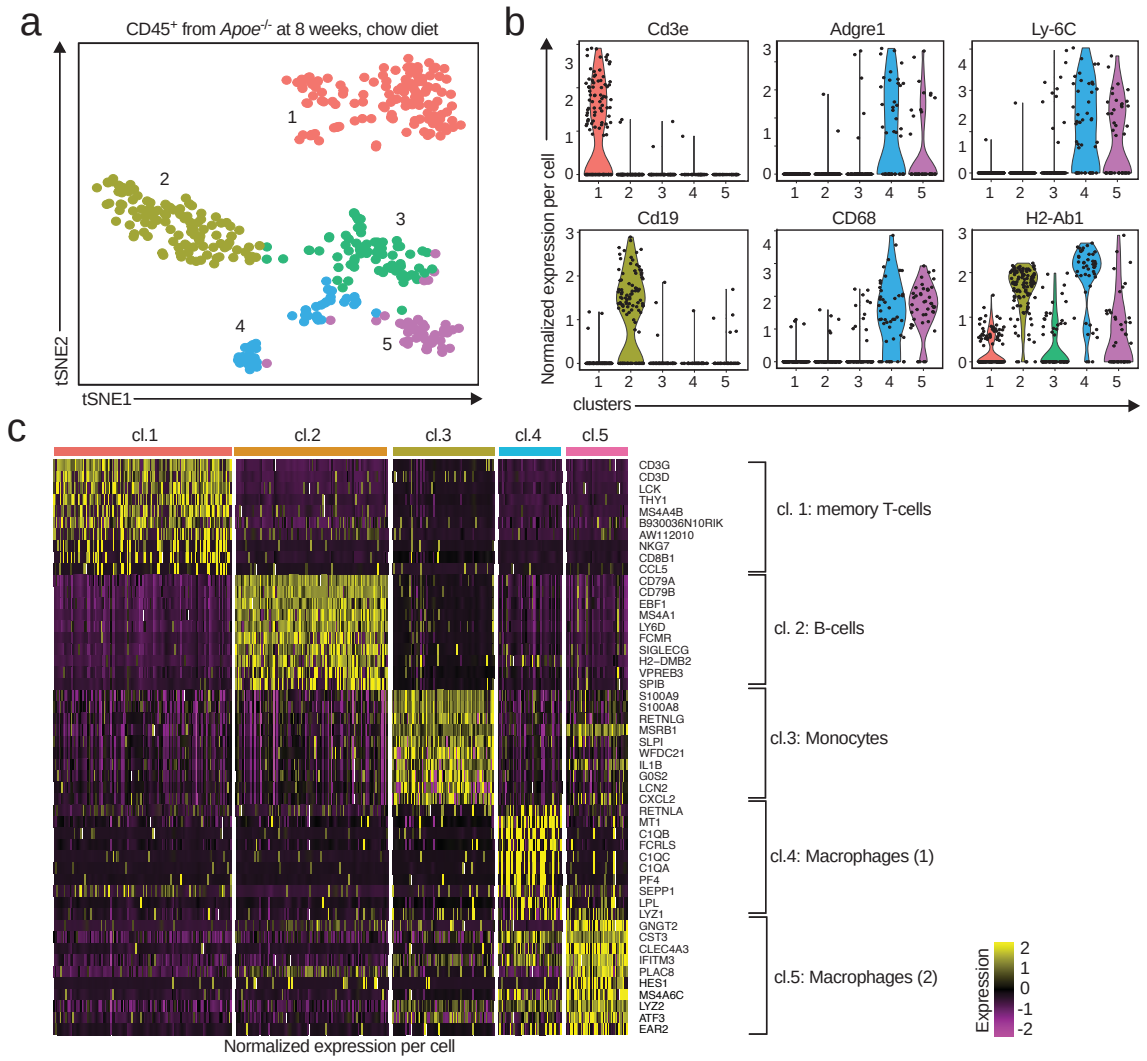

Online Figure VI: Vascular leukocyte subsets identified by scRNAseq in aortas from young, healthy *Apoe*$^{-/-}$ mice. (**a**) Single cell transcriptomes of aortic leukocytes pooled from 10 individual 8-week old *Apoe*$^{-/-}$ mice analyzed with an unsupervised dimensionality reduction algorithm (tSNE) to identify groups of cells with similar gene expression. (**b**) Expression of principal hematopoietic lineage markers in the five identified cell clusters shown as normalized gene expression per cell. (**c**) Top 10 differentially expressed genes among all detected aortic leukocyte clusters. Normalized single cell gene expression is shown.

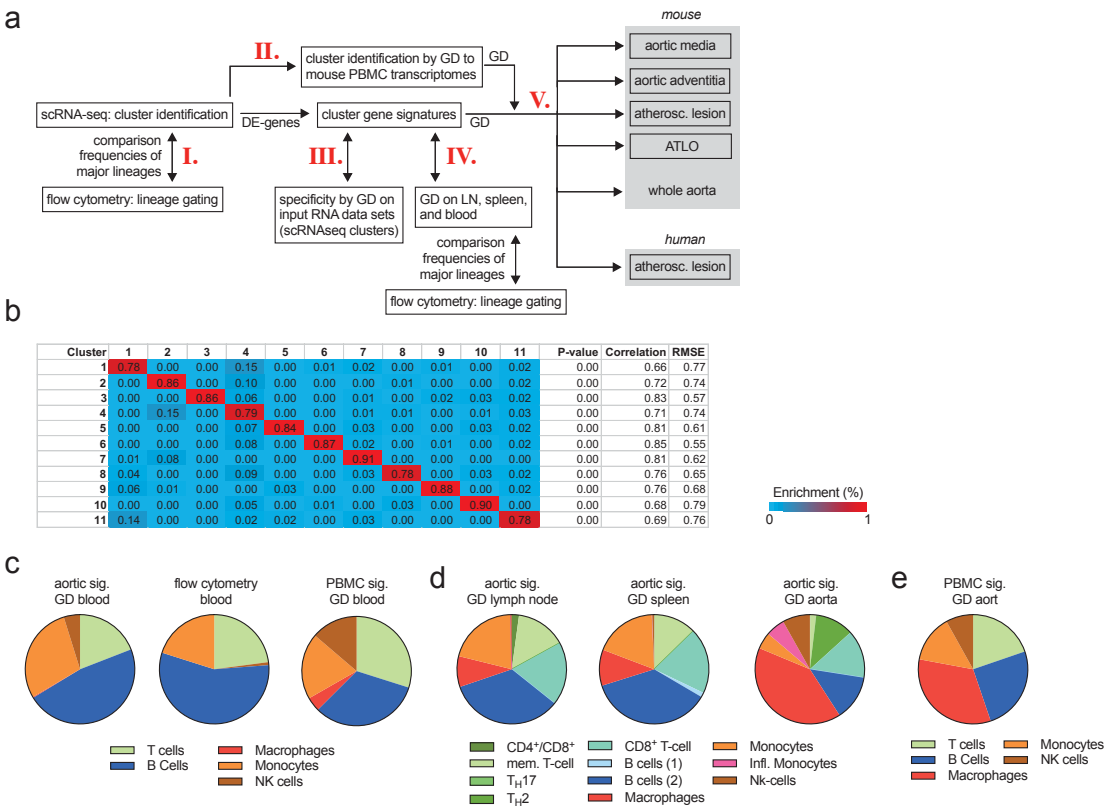

Cluster	1	2	3	4	5	6	7	8	9	10	11	P-value	Correlation	RMSE
1	0.78	0.00	0.00	0.15	0.00	0.01	0.02	0.00	0.01	0.00	0.02	0.00	0.66	0.77
2	0.00	0.86	0.00	0.10	0.00	0.00	0.00	0.01	0.00	0.00	0.02	0.00	0.72	0.74
3	0.00	0.00	0.86	0.06	0.00	0.00	0.01	0.00	0.02	0.03	0.02	0.00	0.83	0.57
4	0.00	0.15	0.00	0.79	0.00	0.00	0.01	0.01	0.00	0.01	0.03	0.00	0.71	0.74
5	0.00	0.00	0.00	0.07	0.84	0.00	0.03	0.00	0.00	0.03	0.02	0.00	0.81	0.61
6	0.00	0.00	0.00	0.08	0.00	0.87	0.02	0.00	0.01	0.00	0.02	0.00	0.85	0.55
7	0.01	0.08	0.00	0.00	0.00	0.00	0.91	0.00	0.00	0.00	0.00	0.00	0.81	0.62
8	0.04	0.00	0.00	0.09	0.00	0.00	0.03	0.78	0.00	0.03	0.02	0.00	0.76	0.65
9	0.06	0.01	0.00	0.00	0.03	0.00	0.00	0.00	0.88	0.00	0.02	0.00	0.76	0.68
10	0.00	0.00	0.00	0.05	0.00	0.01	0.00	0.03	0.00	0.90	0.00	0.00	0.68	0.79
11	0.14	0.00	0.00	0.02	0.02	0.00	0.03	0.00	0.00	0.00	0.78	0.00	0.69	0.76

Online Figure VII: Validation of aortic leukocyte cluster gene signatures. (**a**) An overview of the stepwise strategy exercised during constructing, validating, and applying aortic leukocyte signatures for genetic deconvolution (GD). (**b**) Gene signatures were constructed based on the top 50 highest differentially expressed cluster genes (vs. all other clusters) from the 11 aortic leukocyte clusters. These gene signature (columns) were re-tested for specificity by GD within the average gene expression values from the 11 input clusters (rows). The calculated relative enrichment of cellular events with the tested gene signature within the tested gene expression matrix is shown as % of total signal. Cluster number according to Figure 1. (**c**) To validate the fractions retrieved by the aortic leukocyte signatures (left), we compared these to lineage-frequencies assessed by flow cytometry (middle), and frequencies calculated by a GD of a published mouse PBMC signature[23] (right) within blood leukocytes (middle) and whole blood RNA expression data sets from *Apoe*$^{-/-}$ mice (GSE40156, left and right). (**d**) GD of aortic leukocyte signatures within whole tissue RNA expression data sets from lymph nodes (left), spleen (middle), and whole atherosclerotic aortas from *Apoe*$^{-/-}$ mice (GSE40156). (**e**) A mouse PBMC signature[23] was quantified by a GD within whole aortic tissue RNA expression arrays from *Apoe*$^{-/-}$ mice (GSE40156).

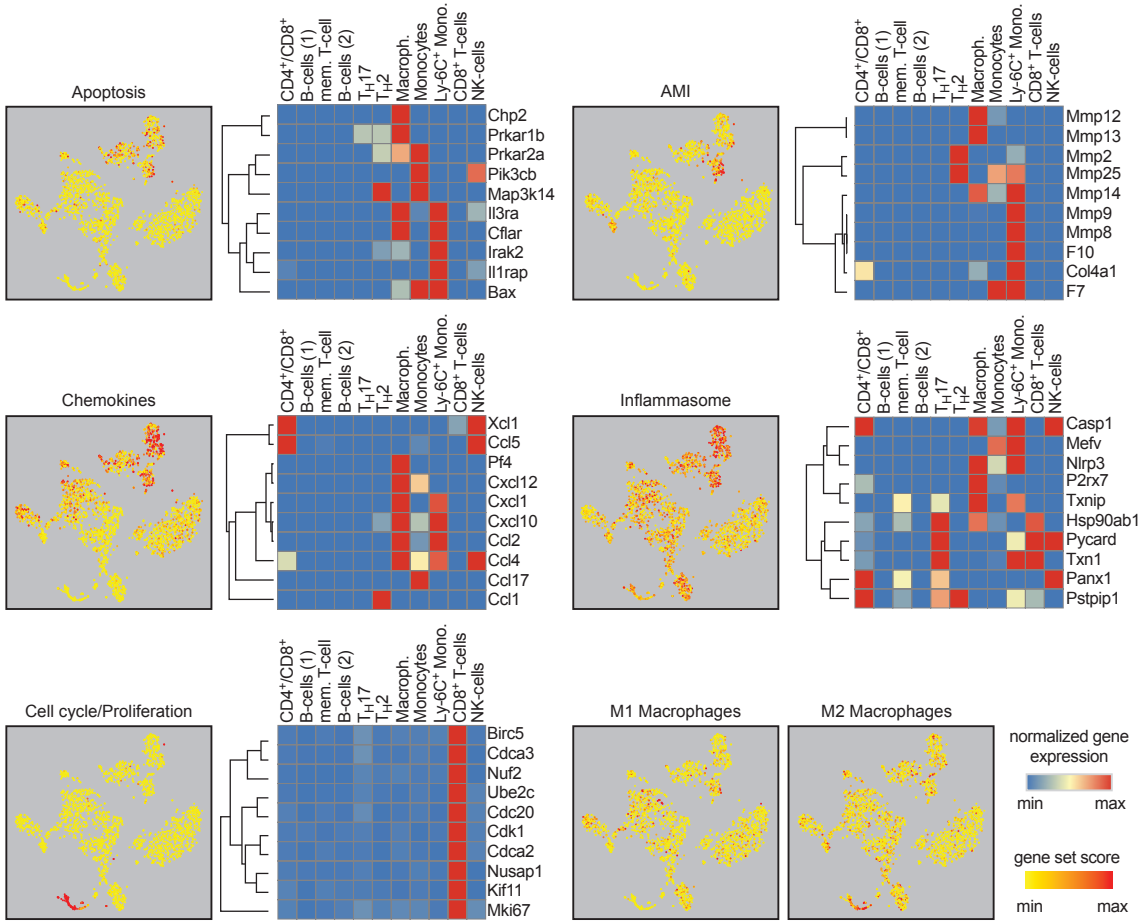

Online Figure VIII: Single cell gene set enrichment in aortic leukocyte clusters. Single cell transcriptomes of the eleven identified leukocyte clusters were analyzed for the enrichment of specific genes and pathways. The expression of genes pertaining to apoptosis, chemokines, the inflammasome, cell cycle/proliferation, M1 macrophage signatures, and M2 macrophage signatures was retrieved and summarized as gene set score (specific enrichment normalized for background) per cell. Gene set scores were overlaid on single cells on a tSNE plot to identify leukocyte clusters with an enrichment of the indicated gene sets (left). The mean expression of key genes within the specific gene set is presented as heatmap with a row min.-max. score (right).

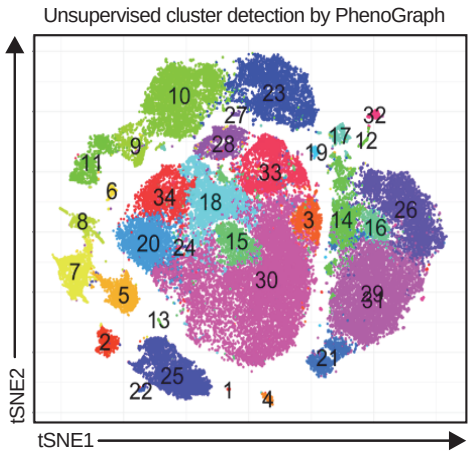

Online Figure IX: Phenotypic clustering of splenocytes in CyTOF/PhenoGraph. A 35-marker pan-leukocyte CyTOF antibody panel (full panel shown in Online Table VI) was used to stain splenocytes ($1x10^6$) from CD45.1 *Apoe*$^{-/-}$ mice. Dimensionality reduction and unsupervised cell cluster detection was performed by PhenoGraph on live, CD45$^+$ pre-gated splenocytes. 34 different splenocyte clusters could be detected, 22 of which were above the frequency cut-off of 1 %. Relative marker expression across clusters is shown in Online Figure X.

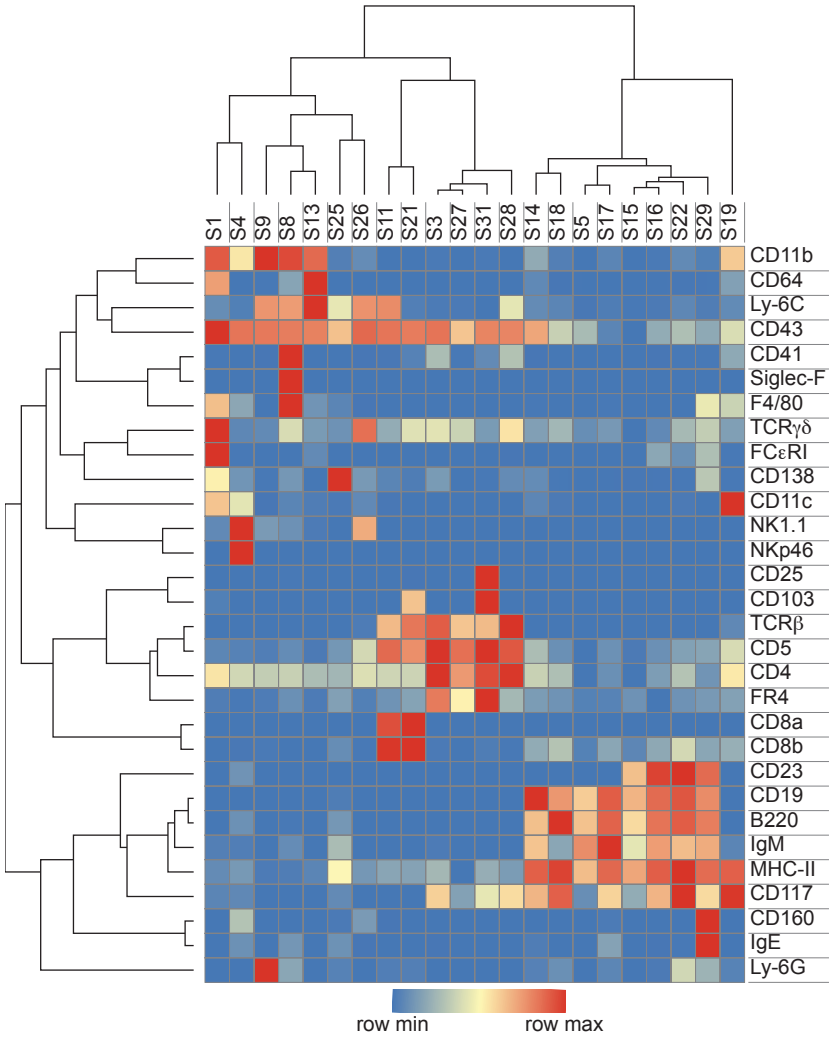

Online Figure X: Heatmap of marker expression by splenocyte clusters in CyTOF/PhenoGraph. A 35-marker pan-leukocyte CyTOF antibody panel (full panel shown in Table S6) was used to stain splenocytes ($1x10^6$) from CD45.1 *Apoe*$^{-/-}$ mice. Dimensionality reduction and unsupervised cell cluster detection was performed by PhenoGraph on live, CD45$^+$ pre-gated splenocytes. Shown here are the 22 clusters above the frequency threshold of 1 %. Cluster names according to Online Figure IX.

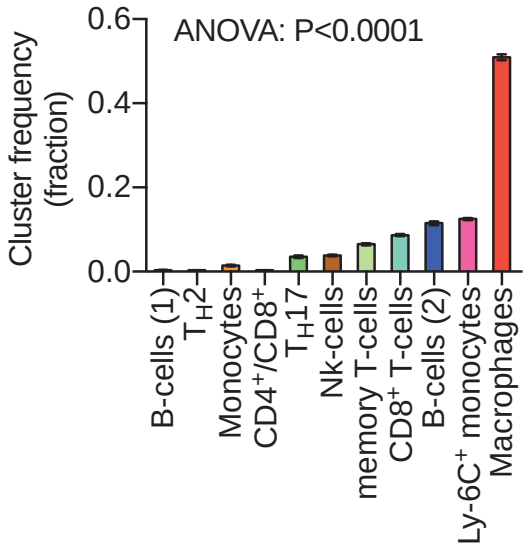

Online Figure XI: Leukocyte composition of human carotid atherosclerotic plaques. A genetic deconvolution of leukocyte cluster gene signatures was performed in a set of bulk mRNA expression data sets of 126 human carotid plaques from the Biobank of Karolinska Endarterectomies (BiKE) to enumerate the relative abundance of cell clusters. The relative frequency of the tested clusters is shown (fraction). Statistical significance was calculated by a one-way ANOVA. Data are presented as mean ± SEM.

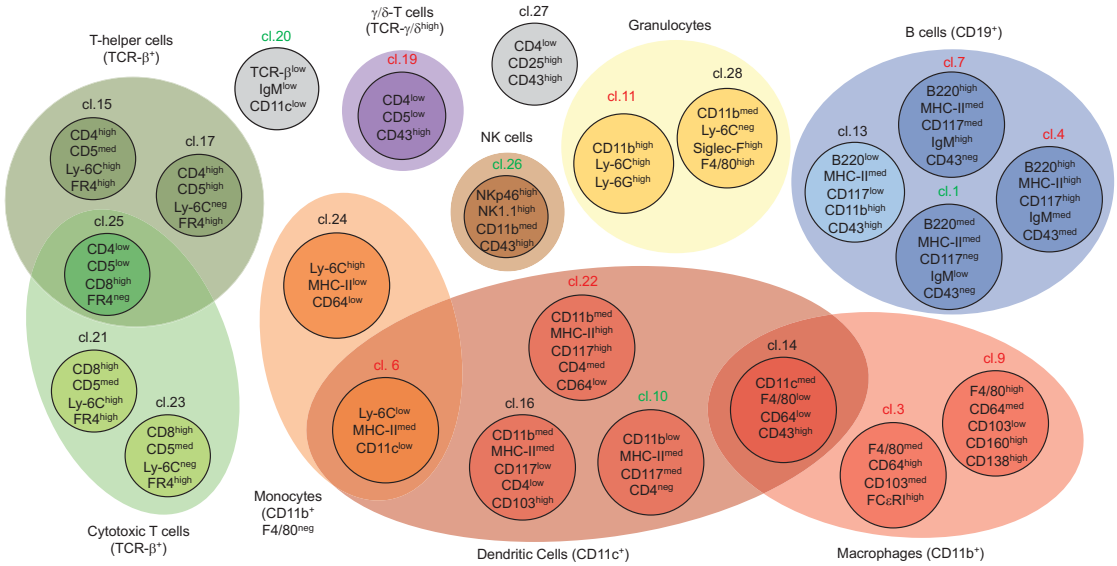

Online Figure XII: Immune cell atlas in atherosclerosis. Cell clusters found in CyTOF of atherosclerotic aortas were grouped for principal hematopoietic lineages (background circles). Key marker expression is shown within schematic cells. Numbers above clusters indicate CyTOF cluster numbers (according to Figure 4). A green colored cluster name indicates a decrease, red color an increase of cluster cell numbers in WD- compared to CD-induced atherosclerosis in *Apoe*$^{-/-}$ mice after 12 weeks of feeding.

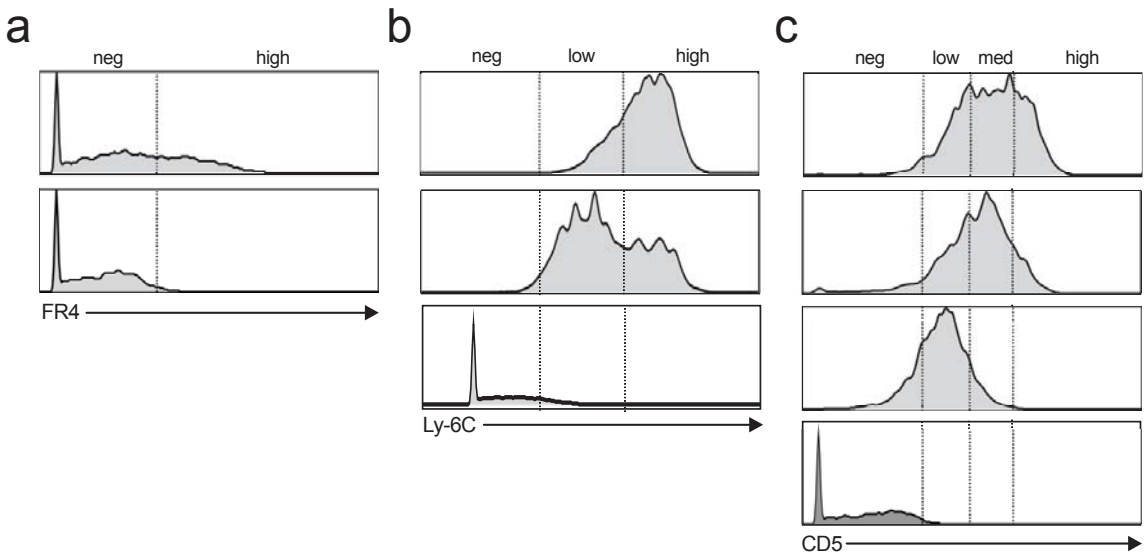

Online Figure XIII: Definition of marker expression categories in CyTOF histograms. Leukocyte clusters retrieved by PhenoGraph were exported and the markers FR4 (a), Ly6-C (b), and CD5 (c) were displayed to demonstrate the amplitude of marker expression across selected clusters. All histograms are normalized to mode.

ONLINE TABLES

Online Table I: Top20 differentially expressed (DE) genes in the scRNAseq-defined leukocyte clusters. All genes were significantly regulated vs. all other clusters (P<0.05)

Cl.1	Cl.2	Cl.3	Cl.4	Cl.5	Cl.6
CCL5	CD741	LEF11	CD743	DNTT	RORA
NKG7	H2-AA1	RPLP1	CD79A3	TCF73	FURIN
AW112010	CD79A1	RPS7	H2-AA3	LDHB	CXCR61
MS4A4B	EBF11	RPLP0	EBF13	LCK4	LMO45
HCST	H2-AB11	RPS23	H2-EB13	CCR9	GATA3
CTSW	H2-EB11	DAPL1	H2-AB13	ENDOU	RAMP3
GZMK	H2-DMB21	TMSB102	H2-DMB23	ARPP21	RGS24
MS4A6B	SERP11	RPS18	MS4A13	CD8B13	NFKB15
CD3G	MEF2C1	RPL12	CD79B1	SOX4	GADD45B
GIMAP4	MS4A11	RPS29	FCMR1	SATB12	CCDC184
CD3D	CD831	RPS15A	MZB11	RAG1	HILPDA3
TMSB10	GM43603	RPL17	MEF2C3	RMND5A	GM20186
FASL	RPS27	RPS191	H2-OB3	RHOH	IL1RL1
RPL13A	SCD1	RPS16	CD833	SPINT2	AREG
LCK	CCR71	RPS3A1	SCD11	AP3S14	ARG1
ITGB1	H2-OB1	RPS6	LY6D3	AQP11	CISH
GRAMD3	FCMR	RPS27A	BANK11	CD8A2	FOSL24
ZFP36L2	RPS19	RPS4X	FCRLA1	CYB5A3	CCR24
SH2D2A	LY6D1	RPS271	CCR73	RAMP14	SAMSN13
CTLA2A	BANK1	RPS14	RPS202	SSBP2	TMEM176

Cl.7	Cl.8	Cl.9	Cl.10	Cl.11
C1QB	CST37	MSRB1	HMGB28	AW1120108
C1QA	GM2A5	CLEC4E	TUBA1B6	KLRB1C
C1QC	PLBD11	TYROBP8	HMGB19	NCR1
SEPP15	IFI305	PRDX53	PTMA3	KLRE1
CTSB6	TYROBP7	CEBPB7	UBE2S6	GZMA1
FTL16	ATOX16	FCER1G8	HMGN25	KLRK11
CTSC6	CD209A	F10	STMN11	KLRI2
LYZ26	CD747	FTL18	TUBB57	IRF87
ITM2B5	SYNGR23	FTH15	H2AFV8	NKG710
CSF1R	IFITM21	LST11	H2AFZ5	TYROBP10
TRF	LGALS37	CSTB8	TOP2A	KLRD12
C3AR1	H2-DMB15	LGALS38	HIST1H2AP	KLRA7
ADGRE1	IFITM36	GNGT24	2810417H1	CAR2
FCGR3	FCER1G7	THBS1	ANP32E9	CCL510
PF4	H2-AB17	IFITM37	BIRC5	FCER1G10
MS4A7	H2-AA7	RNF1492	RRM2	KLRB1A
CD14	H2-EB17	GSR	H2AFX	IL2RB2
CD63	LSP13	TGFBI2	NUSAP1	SERPINB6B
CST36	ALOX5AP1	LYZ28	TMPO	KLRA4
FCER1G6	WFDC171	PSAP7	ANP32B3	CMA1

Online Table II: Fluorochrome-conjugated antibodies used for conventional flow cytometry

Target	Fluorochrome	Clone	Catalog #	Company
CD45	PerCP	30-F11	103130	Biolegend
CD11b	PE-Cy7	M1/70	101216	Biolegend
CD117	APC	2B8	105812	Biolegend
CD19	APC-Cy7	6D5	115530	Biolegend
FCεRI	AF700	MAR-1	134324	Biolegend
TCR-γ/δ	FITC	GL3	118106	Biolegend
CD8a	BV421	53-6.7	100738	Biolegend
CD11c	BV605	N418	117334	Biolegend
NK1.1	BV650	PK136	108736	Biolegend
TCR-β	BV711	H57-597	109243	Biolegend
GR1	BV786	RB6-8C5	740850	BD Biosciences
CD4	PE/Dazzle 594	GK1.5	100456	Biolegend
F4/80	PE	BM8	123110	Biolegend
Viability/Ghost	BV510		13-0870-T500	Tonbo Biosciences

Online Table III: Cluster frequency changes in *Apoe*$^{-/-}$ and *Ldlr*$^{-/-}$ mice (% of all leukocytes)

Lineage	***Ldlr*$^{-/-}$ on CD**	***Ldlr*$^{-/-}$ on HFD**	***Apoe*$^{-/-}$ on CD**	***Apoe*$^{-/-}$ on WD**
NK-cells	1.7	2.1	2.4	1.6
Macrophages	13.6	27.0	4.9	9.6
B-cells	24.4	4.0	21.9	27.2
Myeloid cells	6.2	21.1	10.3	12.6
T-cells	54.1	45.8	60.6	49.0

Online Table IV A: Top20 up-regulated genes between leukocytes from WD-and CD-fed *Apoe*$^{-/-}$ in the same cluster. All genes were significantly regulated vs. all other clusters (P<0.05)

Cl.1	Cl.2	Cl.3	Cl.4	Cl.5	Cl.6
GIMAP7	KPNA1	ANKRD11	LUC7L3	APOBEC3	SRRD
ATRX	MAFG	H2-DMA	SUSD6	FBXO33	TSG101
CCL5	NDUFA3	BCCIP	FAM49B	C1GALT1	PTPRCAP
MDP1	RNF167	MIEN1	EMC3	NEU1	2810474O1
NDUFA5	LGMN	STAT5B	UBE2B	MAP2K1	AQP3
BCL11B	SMARCA5	SERP1	RTCB	PDLIM5	ATG3
MED28	PCMTD1	FAM32A	IL10RA	HS2ST1	URI1
DDIT3	MRPS16	PKN2	LSM12	FAM192A	TRAM1
CDKN2AIP	SCAND1	SET	38961	TRAPPC12	40057
IFNGR1	DDX21	SELK	BOLA2	BANP	PDCD1LG2
DPCD	CAPZB	USMG5	EIF5	CTLA2A	USP1
HIST1H2AP	LAMTOR5	ABCG1	FCRL1	H2-Q7	GM26699
CHD1	TIA1	ZCCHC7	MRPL51	PHLDA1	AIG1
BCL2	SERPINA3	PHF5A	YWHAG	SLC7A11	ANKRD11
SMAP1	FAM50A	PLAUR	TMED10	AKAP9	1110008F13
LILR4B	TRAPPC5	HSP90B1	UQCR10	IFNAR1	TTC14
CD8A	SBDS	GPR18	EIF3C	EIF4E	TPR
CTLA2A	HEXA	DENR	TSIX	MYB	5430421N2
PLAC8	TRP53	GPBP1	ZBTB20	LY6K	SOAT1
CCL4	WNK1	PSMA4	FOXP1	NKG7	CD74

Cl.7	Cl.8	Cl.9	Cl.10	Cl.11
FUNDC1	SET	MRPL15	UTP3	TAF5L
IFIH1	SAFB2	PYCARD	SSSCA1	CTR9
AMD1	PLK2	MGST1	FAM111A	PARK7
FGL2	UQCRQ	FCGR1	GEMIN7	MED28
PHF11D	NDUFB3	HILPDA	RFWD2	PLAC8
GM4955	KLF13	GM9733	PUM1	SSR2
CCND1	TSPAN13	NDUFB7	LSM12	MYO1G
MS4A6C	KLRD1	SPG21	UQCRFS1	KRTCAP2
STMN1	OGFRL1	ROMO1	GIMAP4	MED10
IFI47	NCOR1	HSP90B1	TEX261	CBFB
BST2	LY6A	JUND	TKT	LSM6
LY6A	ST13	RHOB	TOX	DNAJC5
RTP4	IL21R	BASP1	HIST1H3B	EIF2A
LY6E	PITPNA	P4HB	NSUN2	PBDC1
JUN	PCYT1A	LY6C2	NDUFAF3	REL
CCL12	TBC1D4	OSM	GOLGA7	PCNA
CITED2	CD7	CHIL3	HSPH1	ERGIC3
IFI27L2A	GNGT2	INHBA	PURB	RFC2
CCL8	IFITM1	CCL2	G3BP1	LGALS3
SPP1	PLAC8	CCL4	HSPE1	TCEB1

Online Table IV B: Top20 down-regulated genes between leukocytes from WD-and CD-fed *Apoe*$^{-/-}$ in the same cluster. All genes were significantly regulated vs. all other clusters (P<0.05)

Cl.1	Cl.2	Cl.3	Cl.4	Cl.5	Cl.6
GM26917	RPS27RT	RPS27RT	GM26917	AY036118	IFI27L2A
RPL6L	GM6133	RPL6L	CST3	GM10036	GM26917
RPS27RT	AY036118	RPL13-PS3	RPS27RT	RPS27RT	RPS12-PS3
RPL13-PS3	GM42418	GM26917	GM9493	GM6133	PFN1
GM6133	RPL36-PS3	GM6133	GM6133	GM26917	GEM
GM9493	WDR89	AY036118	GM42418	GM9844	RPL13-PS3
WDR89	GM26917	GM9493	RPL6L	GM11808	GM42418
GM8730	RPL27-PS3	WDR89	RPL13-PS3	LRRC58	WDR89
GM42418	GM9493	GM11808	GM11808	RPL6L	GM6133
GM11808	RPS26-PS1	GM9844	WDR89	PFN1	AY036118
GM9843	RPL6L	RPL36-PS3	GM9843	RPL13-PS3	RPL9-PS6
RPL23A-	RPL13-PS3	RPS26-PS1	AY036118	RPL23A-	GM11808
PFN1	GM11808	RPL23A-	RPL27-PS3	CCM2	GM10036
AY036118	GM9843	RPS12-PS3	GM9844	TMEM167	RPL36-PS3
RPL27-PS3	CXCR4	GM9843	PFN1	GM9843	RPS27RT
GM2000	GM9844	GM8797	RPL10-PS3	GM5914	RPL27-PS3
GM10036	SLC16A6	PFN1	GM10263	GM9493	GM9493
RPL36-PS3	PFN1	RPL9-PS6	RPS26-PS1	WDR89	CD274
RPS12-PS3	SZRD1	GM8186	RPS12-PS3	TOR1AIP1	GM9843
CST3	RPS12-PS3	GM42418	RPL9-PS6	IRF3	RPL23A-

Cl.7	Cl.8	Cl.9	Cl.10	Cl.11
LYZ1	LYZ1	EAR2	CXCL2	GM42418
GM42418	RPS27RT	SPN	AY036118	LMO4
RPS27RT	WDR89	HES1	PRKCSH	ZEB2
GM26917	CD14	RPS27RT	GM26917	COQ10B
AY036118	GM11808	ACE	GSTP1	BANF1
GM9843	GM9843	GM6133	VDAC3	GEM
GM9493	RPS12-PS3	RPL27-PS3	TUBB2B	RPL13-PS3
GM6133	RPL6L	ADGRE4	H1F0	RPS27RT
RPL6L	GM6133	CD300E	IER5	RNASET2B
GM10116	AY036118	GM9843	KPNA2	RAB7
RPS12-PS3	GM9493	ANKRD44	TSC22D3	HEXB
GM10036	RPL36-PS3	LST1	ZFP36	AY036118
GM8797	RPL10-PS3	RPL13-PS3	RNASET2A	RPL6L
WDR89	RPL13-PS3	RPL10-PS3	PFN1	CHST12
PER1	RPL9-PS6	EIF4A2	CCR9	ZBTB25
RPL36-PS3	GM8730	CDC26	GM9843	NDEL1
BATF	TPPP3	GM26917	GM9493	CD300LF
CXCR4	HSPA1B	RPL23A-	GM8186	WDR89
NLRP3	MAFB	POU2F2	RPL6L	TSC22D3
RGL1	GM9844	FMNL1	HMGB3	IMPDH2

Online Table V: Top10 enriched pathways in leukocyte cluster

Cl.1	Cl.2	Cl.3	Cl.4
Th1 Pathway	**R**egulation of Actin-based Motility by Rho	**P**rotein Ubiquitination Pathway	**P**entose Phosphate Pathway (Oxidative Branch)
Th1 and Th2 Activation Pathway	**C**ell Cycle: G2/M DNA Damage Checkpoint Regulation	**A**ldosterone Signaling in Epithelial Cells	**P**rotein Ubiquitination Pathway
Primary Immunodeficiency Signaling	**E**RK/MAPK Signaling	**U**nfolded protein response	**P**entose Phosphate Pathway
PCP pathway	**S**ystemic Lupus Erythematosus Signaling	**P**rostate Cancer Signaling	**B**ER pathway
Calcium-induced Apoptosis	**I**nduction of Apoptosis by HIV1	**A**ryl Hydrocarbon Receptor Signaling	**M**ismatch Repair in Eukaryotes
CD40 Signaling	**M**yc Mediated Apoptosis Signaling	**T**h2 Pathway	**G**ADD45 Signaling
Communication between Innate and Adaptive Immune Cells	**P**rotein Kinase A Signaling	**e**NOS Signaling	
G-Protein Coupled Receptor Signaling	**H**IPPO signaling	**T**h1 and Th2 Activation Pathway	
iCOS-iCOSL Signaling in T Helper Cells	**S**umoylation Pathway	**I**ntegrin Signaling	
Atherosclerosis Signaling	**C**holecystokinin/Gastrin-mediated Signaling	**E**IF2 Signaling	

Cl.5	Cl.6	Cl.7	Cl.8
Regulation of Actin-based Motility by Rho	**P**EDF Signaling	**H**ypoxia Signaling in the Cardiovascular System	**G**lutamine Biosynthesis I
DNA Methylation and Transcriptional Repression Signaling	**V**itamin-C Transport	**N**eurotrophin/TRK Signaling	**I**L-10 Signaling
Sirtuin Signaling Pathway	**R**etinoic acid Mediated Apoptosis Signaling	**C**ircadian Rhythm Signaling	**H**eme Degradation
Trehalose Degradation II (Trehalase)	**E**phrin B Signaling	**F**GF Signaling	**L**actose Degradation III
PI3K/AKT Signaling	**M**itochondrial Dysfunction	**P**rostate Cancer Signaling	**C**DK5 Signaling
Integrin Signaling	**A**ntioxidant Action of Vitamin C	**N**RF2-mediated Oxidative Stress Response	**S**phingomyelin Metabolism
Aspartate Degradation II	**O**xidative Phosphorylation	**p**38 MAPK Signaling	**p**53 Signaling
Actin Cytoskeleton Signaling	**P**yrimidine Ribonucleotides Interconversion	**A**MPK Signaling	**G**ADD45 Signaling
Actin Nucleation by ARP-WASP Complex	**P**yrimidine Ribonucleotides De Novo Biosynthesis	**E**strogen-Dependent Breast Cancer Signaling	**H**epatic Cholestasis
autophagy	**A**scorbate Recycling (Cytosolic)	**M**olecular Mechanisms of Cancer	**M**itochondrial Dysfunction

Cl.9	Cl.10	Cl.11
B Cell Receptor Signaling	**N**ur77 Signaling in T Lymphocytes	**R**emodeling of Epithelial Adherens Junctions
Leukocyte Extravasation Signaling	**C**alcium-induced T Lymphocyte Apoptosis	**R**egulation of Actin-based Motility by Rho
Osteoarthritis Pathway	**R**egulation of IL-2 Expression in Activated and Anergic T Lymphocytes	**B**reast Cancer Regulation by Stathmin1
Notch Signaling	**G**erm Cell-Sertoli Cell Junction Signaling	**A**ctin Nucleation by ARP-WASP Complex
Protein Kinase A Signaling	**R**egulation of Actin-based Motility by Rho	**R**hoA Signaling
Th2 Pathway	**S**irtuin Signaling Pathway	**P**hospholipase C Signaling
Regulation of eIF4 and p70S6K Signaling	**R**ole of NFAT in Regulation of the Immune Response	**P**hagosome Maturation
Wnt/β-catenin Signaling	**R**ole of NFAT in Cardiac Hypertrophy	**S**ignaling by Rho Family GTPases
Calcium-induced T Lymphocyte Apoptosis	**C**ardiac Hypertrophy Signaling	**C**dc42 Signaling
Mitotic Roles of Polo-Like Kinase	**P**hospholipase C Signaling	**P**rotein Kinase A Signaling

Online Table VI: Metal-conjugated antibodies used for CyTOF (mouse)

Target	Metal	Clone	Catalog #	Company
CD45	89Y	30-F11	3089005B	Fluidigm
Ly-6C	141Pr	HK1.4	128002	Biolegend
CD11c	142Nd	N418	3142003B	Fluidigm
TCR-β	143Nd	H57-597	3143010B	Fluidigm
CD41	144Nd	MWReg30	133902	Biolegend
CD45.1	145Nd	A20	110702	Biolegend
CD5	146Nd	53-7.3	3146012B	Fluidigm
CD11b	148Nd	M1/70	101202	Biolegend
CD19	149Sm	6D5	115502	Biolegend
CD64	150Nd	X54-5/7.1	139302	Biolegend
CD25	151Eu	3C7	3151007B	Fluidigm
Siglec-F	152Sm	1RNM44N	14-1702-82	eBioscience
CD8a	153Eu	53-6.7	3153012B	Fluidigm
TER-119	154Sm	TER-119	3154005B	Fluidigm
FR4	155Gd	TH6	125102	Biolegend
CD103	156Gd	2E7	121402	Biolegend
TCR-γ/δ	159Tb	GL3	3159012B	Fluidigm
B220	160Gd	RA3-6B2	3160012B	Fluidigm
FCεRI	161Dy	Mar-1	134302	Biolegend
CD23	163Dy	B3B4	101602	Biolegend
NK1.1	164Dy	PK136	108702	Biolegend
CD160	165Ho	7H1	143002	Biolegend
F4/80	166Er	BM8	123102	Biolegend
IgE	168Er	RME-1	406902	Biolegend
IgM	169Tm	RMM-1	406502	Biolegend
CD138	170Er	281-2	142502	Biolegend
CD43	171Yb	S11	143202	Biolegend
CD4	172Yb	RM4-5	3172003B	Fluidigm
CD117	173Yb	2B8	3173004B	Fluidigm
MHC-II	174Yb	M5/114.15.2	3174003B	Fluidigm
Ly-6G	175Lu	1A8	127602	Biolegend
NKp46	176Er	29A1.4	3167008B	Fluidigm
CD8b	176Yb	YTS1567.7	126602	Biolegend
DNA	191Ir	n/a	201192B	Fluidigm
DNA	193Ir	n/a	201192B	Fluidigm
Viability	195Pt	n/a	201064	Fluidigm

Online Table VII: Aortic leukocyte clusters above the frequency cutoff of 1% in chow diet and western diet fed *Apoe*$^{-/-}$ mice assessed by CyTOF.

Cl.	Cluster markers	Frequency among aortic, living leukocytes (%)		p
		Chow diet (n=3)	Western diet (n=7)	
1	CD19^{med}, B220^{med}, MHC-II^{med}, IgM^{low}, CD43^{neg}, CD117^{neg}	23.75 ± 5.09	0.76 ± 0.14	****
3	CD64^{high}, FCεRI^{high}, CD11b^{med}, CD103^{med}, CD11c^{neg}, F4/80^{med}, MHC-II^{med}	7.30 ± 0.34	16.69 ± 2.34	*
4	CD19^{high}, B220^{high}, MHC-II^{high}, IgM^{med}, CD23^{high}, CD138^{neg}, CD43^{med}, CD117^{high}	0.33 ± 0.18	1.41 ± 0.36	ns
6	Ly6C^{low}, CD11b^{med}, CD11c^{low}, MHC-II^{med}	2.30 ± 0.26	4.52 ± 0.57	*
7	B220^{high}, CD19^{med}, IgM^{high}, MHC-II^{med}, CD23^{neg}, CD138^{neg}, CD117^{med}, CD43^{neg}	3.61 ± 0.53	10.12 ± 2.08	ns
9	F4/80^{high}, CD11c^{neg}, CD64^{med}, MHC-II^{med}, CD138^{high}, CD160^{high}, CD103^{low}	0.65 ± 0.26	3.32 ± 0.47	**
10	CD11c^{high}, F4/80^{neg}, CD11b^{low}, CD138^{neg}, MHC-II^{med}, CD117^{med}, CD4^{neg}	4.75 ± 0.93	3.64 ± 0.45	ns
11	CD11b^{high}, Ly-6C^{high}, Ly-6G^{high}, NK1.1^{low}	2.01 ± 0.17	6.90 ± 1.17	*
13	CD11b^{high}, B220^{low}, CD19^{high}, IgM^{high}, MHC-II^{med}, CD23^{neg}, CD138^{neg}, CD43^{high}, CD117^{low}	2.89 ± 0.30	1.26 ± 0.19	**
14	CD43^{high}, CD11c^{med}, CD11b^{med}, CD64^{low}, F4/80^{low}	4.03 ± 1.05	4.54 ± 0.59	ns
15	TCR-β^{high}, CD4^{high}, CD5^{med}, CD43^{high}, FR4^{high}, Ly-6C^{high}	4.30 ± 2.07	3.42 ± 0.66	ns
16	CD11c^{high}, CD11b^{med}, CD103^{high}, MHC-II^{med}, CD4^{low}, FR4^{high}, CD117^{low}	0.27 ± 0.16	1.24 ± 0.21	*
17	TCR-β^{high}, CD4^{high}, CD5^{high}, CD43^{high}, FR4^{high}, Ly-6C^{neg}	5.60 ± 1.10	6.91 ± 0.43	ns
19	TCR-γ/δ^{high}, CD4^{low}, CD5^{low}, CD43^{high}	1.07 ± 0.33	3.36 ± 0.35	**
20	TCR-β^{low}, IgM^{low}, CD11c^{low}	3.31 ± 0.04	0.14 ± 0.08	****
21	TCR-β^{high}, CD8^{high}, CD4^{low}, CD5^{med}, Ly-6C^{high}, FR4^{high}	3.54 ± 1.39	5.12 ± 0.74	ns
22	CD11c^{high}, F4/80^{neg}, CD11b^{med}, CD138^{low}, MHC-II^{high}, CD117^{high}, CD64^{low}, CD4^{low}	0.32 ± 0.09	3.48 ± 0.42	**
23	TCR-β^{high}, CD8^{high}, CD4^{low}, CD5^{med}, FR4^{high}, Ly-6C^{neg}	3.68 ± 2.11	4.27 ± 1.10	ns
24	Ly6-C^{high}, CD11b^{med}, CD64^{low}, MHC-II^{low}	4.72 ± 1.08	3.91 ± 0.54	ns
25	CD4^{low}, CD8^{high}, CD5^{low}, TCR-β^{neg}	4.83 ± 0.76	5.65 ± 1.75	ns
26	NK1.1^{high}, NKp46^{high}, CD23^{high}, CD11b^{med}, CD43^{high}	5.44 ± 1.27	1.00 ± 0.10	***
27	TCR-β^{neg}, CD4^{low}, CD25^{high}, CD43^{high}	3.90 ± 0.29	3.14 ± 0.39	ns
28	CD11b^{med}, Ly-6C^{neg}, Siglec-F^{high}, F4/80^{high}	1.51 ± 0.41	1.86 ± 0.27	ns
	SUM	92.56 ± 4.20	96.66 ± 0.57	ns

'Cl.' indicates cluster, 'p' indicates P-value. Data are presented as mean ± standard error mean. Statistical significance between mild atherosclerosis (chow diet fed *Apoe*$^{-/-}$ mice) and advanced atherosclerosis (western diet) for each of the subsets was calculated by a two tailed, unpaired T-test. *p<0.05, **p<0.01, ***p<0.001, ****p<0.0001, ns: not significant. Clusters 2, 5, 8, 12, 18 are not listed because their frequency was under the 1% threshold.

Online Table VIII: Fluorochrome-conjugated antibodies used for intracellular cytokine staining flow cytometry

Target	Fluorochrome	Clone	Catalog #	Company
CD45	AF700	30-F11	103128	Biolegend
CD19	BV711	6D5	115555	Biolegend
CD43	FITC	S11	143203	Biolegend
B220	BV650	RA3-6B2	103241	Biolegend
IL-10	BV421	JES5-16E3	505021	Biolegend
IL-4	PE-Cy7	11B11	504118	Biolegend
IFN-γ	PerCp-Cy5.5	XMG1.2	505281	Biolegend
GM-CSF	APC	MP1-22E9	505414	Biolegend
CCL5	PE	2E9/CCL5	149104	Biolegend
Viability/Ghost	BV510		13-0870-T500	Tonbo Biosciences

Online Table IX: Metal-conjugated antibodies used for CyTOF (human)

Target	Metal	Clone	Company	Catalog #
CD1c	141Pr	L161	Biolegend	331502
CD19	142Nd	HIB19	Fluidigm	3142001B
CD127 (IL-7Ra)	143Nd	A019D5	Fluidigm	3143012B
CD15 (SSEA-1)	144Nd	W6D3	Fluidigm	3144019B
CD4	145Nd	RPA-T4	Fluidigm	3145001B
CD8a	146Nd	RPA-T8	Fluidigm	3146001B
CD303 (BDCA2)	147Sm	201A	Fluidigm	3147009B
CD45RO	149Sm	UCHL1	Fluidigm	3149001B
CD123 (IL-3R)	151Eu	6H6	Fluidigm	3151001B
CD36	152Sm	5-271	Fluidigm	3152007B
CD45RA	153Eu	HI100	Fluidigm	3153001B
CD3	154Sm	UCHT1	Fluidigm	3154003B
CD27	155Gd	L128	Fluidigm	3155001B
CD169 (Siglec-1)	158Gd	7-239	Fluidigm	3158027B
CD11c	159Tb	Bu15	Fluidigm	3159001B
CD14	160Gd	M5E2	Fluidigm	3160001B
CD69	162Dy	FN50	Fluidigm	3162001B
Siglec 8	164Dy	7C9	Fluidigm	3164017B
CD16	165Ho	3G8	Fluidigm	3165001B
IgD	166Er	IA6-2	Biolegend	348202
CD197 (CCR7)	167Er	G043H7	Fluidigm	3167009A
CD25 (IL-2R)	169Tm	2A3	Fluidigm	3169003B
CD20	171Yb	2H7	Fluidigm	3171012B
CD38	172Yb	HIT2	Fluidigm	3172007B
HLA-DR	174Yb	L243	Fluidigm	3174001B
CD56 (NCAM)	176Yb	NCAM16.2	Fluidigm	3176008B
CD11b (Mac-1)	209Bi	ICRF44	Fluidigm	3209003B
CD45	89Y	HI30	Fluidigm	3089003B

ONLINE REFERENCES

1. Galkina E, Kadl A, Sanders J, Varughese D, Sarembock IJ, Ley K. Lymphocyte recruitment into the aortic wall before and during development of atherosclerosis is partially l-selectin dependent. *J Exp Med*. 2006;203:1273-1282

2. Finck R, Simonds EF, Jager A, Krishnaswamy S, Sachs K, Fantl W, Pe'er D, Nolan GP, Bendall SC. Normalization of mass cytometry data with bead standards. *Cytometry A*. 2013;83:483-494

3. van der Maaten L, Hinton, G. Visualizing data using t-sne. *Journal of Machine Learning Research*. 2008;9 2579-2605

4. Chen H, Lau MC, Wong MT, Newell EW, Poidinger M, Chen J. Cytofkit: A bioconductor package for an integrated mass cytometry data analysis pipeline. *PLoS Comput Biol*. 2016;12:e1005112

5. Zheng GX, Terry JM, Belgrader P, Ryvkin P, Bent ZW, Wilson R, Ziraldo SB, Wheeler TD, McDermott GP, Zhu J, Gregory MT, Shuga J, Montesclaros L, Underwood JG, Masquelier DA, Nishimura SY, Schnall-Levin M, Wyatt PW, Hindson CM, Bharadwaj R, Wong A, Ness KD, Beppu LW, Deeg HJ, McFarland C, Loeb KR, Valente WJ, Ericson NG, Stevens EA, Radich JP, Mikkelsen TS, Hindson BJ, Bielas JH. Massively parallel digital transcriptional profiling of single cells. *Nat Commun*. 2017;8:14049

6. Dobin A, Davis CA, Schlesinger F, Drenkow J, Zaleski C, Jha S, Batut P, Chaisson M, Gingeras TR. Star: Ultrafast universal rna-seq aligner. *Bioinformatics*. 2013;29:15-21

7. Hong Y, Kwong S. Learning assignment order of instances for the constrained k-means clustering algorithm. *IEEE Trans Syst Man Cybern B Cybern*. 2009;39:568-574

8. Satija R, Farrell JA, Gennert D, Schier AF, Regev A. Spatial reconstruction of single-cell gene expression data. *Nat Biotechnol*. 2015;33:495-502

9. Chinrungrueng C, Sequin CH. Optimal adaptive k-means algorithm with dynamic adjustment of learning rate. *IEEE Trans Neural Netw*. 1995;6:157-169

10. Huang da W, Sherman BT, Lempicki RA. Systematic and integrative analysis of large gene lists using david bioinformatics resources. *Nat Protoc*. 2009;4:44-57

11. Kramer A, Green J, Pollard J, Jr., Tugendreich S. Causal analysis approaches in ingenuity pathway analysis. *Bioinformatics*. 2014;30:523-530

12. Reich M, Liefeld T, Gould J, Lerner J, Tamayo P, Mesirov JP. Genepattern 2.0. *Nat Genet*. 2006;38:500-501

13. Subramanian A, Tamayo P, Mootha VK, Mukherjee S, Ebert BL, Gillette MA, Paulovich A, Pomeroy SL, Golub TR, Lander ES, Mesirov JP. Gene set

enrichment analysis: A knowledge-based approach for interpreting genome-wide expression profiles. *Proc Natl Acad Sci U S A*. 2005;102:15545-15550

14. Lee K, Santibanez-Koref M, Polvikoski T, Birchall D, Mendelow AD, Keavney B. Increased expression of fatty acid binding protein 4 and leptin in resident macrophages characterises atherosclerotic plaque rupture. *Atherosclerosis*. 2013;226:74-81

15. Tirosh I, Izar B, Prakadan SM, Wadsworth MH, 2nd, Treacy D, Trombetta JJ, Rotem A, Rodman C, Lian C, Murphy G, Fallahi-Sichani M, Dutton-Regester K, Lin JR, Cohen O, Shah P, Lu D, Genshaft AS, Hughes TK, Ziegler CG, Kazer SW, Gaillard A, Kolb KE, Villani AC, Johannessen CM, Andreev AY, Van Allen EM, Bertagnolli M, Sorger PK, Sullivan RJ, Flaherty KT, Frederick DT, Jane-Valbuena J, Yoon CH, Rozenblatt-Rosen O, Shalek AK, Regev A, Garraway LA. Dissecting the multicellular ecosystem of metastatic melanoma by single-cell rna-seq. *Science*. 2016;352:189-196

16. Newman AM, Liu CL, Green MR, Gentles AJ, Feng W, Xu Y, Hoang CD, Diehn M, Alizadeh AA. Robust enumeration of cell subsets from tissue expression profiles. *Nat Methods*. 2015;12:453-457

17. Zhong Y, Wan YW, Pang K, Chow LM, Liu Z. Digital sorting of complex tissues for cell type-specific gene expression profiles. *BMC Bioinformatics*. 2013;14:89

18. Rahmani E, Zaitlen N, Baran Y, Eng C, Hu D, Galanter J, Oh S, Burchard EG, Eskin E, Zou J, Halperin E. Sparse pca corrects for cell type heterogeneity in epigenome-wide association studies. *Nat Methods*. 2016;13:443-445

19. Liebner DA, Huang K, Parvin JD. Mmad: Microarray microdissection with analysis of differences is a computational tool for deconvoluting cell type-specific contributions from tissue samples. *Bioinformatics*. 2014;30:682-689

20. Abbas AR, Wolslegel K, Seshasayee D, Modrusan Z, Clark HF. Deconvolution of blood microarray data identifies cellular activation patterns in systemic lupus erythematosus. *PLoS One*. 2009;4:e6098

21. Gong T, Hartmann N, Kohane IS, Brinkmann V, Staedtler F, Letzkus M, Bongiovanni S, Szustakowski JD. Optimal deconvolution of transcriptional profiling data using quadratic programming with application to complex clinical blood samples. *PLoS One*. 2011;6:e27156

22. Shen-Orr SS, Tibshirani R, Khatri P, Bodian DL, Staedtler F, Perry NM, Hastie T, Sarwal MM, Davis MM, Butte AJ. Cell type-specific gene expression differences in complex tissues. *Nat Methods*. 2010;7:287-289

23. Chen Z, Huang A, Sun J, Jiang T, Qin FX, Wu A. Inference of immune cell composition on the expression profiles of mouse tissue. *Sci Rep*. 2017;7:40508

24. Folkersen L, Persson J, Ekstrand J, Agardh HE, Hansson GK, Gabrielsen A, Hedin U, Paulsson-Berne G. Prediction of ischemic events on the basis of

transcriptomic and genomic profiling in patients undergoing carotid endarterectomy. *Mol Med*. 2012;18:669-675